J. Plasma Physics (2012), vol. 78, part 4, pp. 401–412. © Cambridge University Press 2012
doi:10.1017/S0022377812000232

Simulations of efficient laser wakefield accelerators from 1 to 100 GeV

M. TZOUFRAS[1], C. HUANG[2], J. H. COOLEY[2], F. S. TSUNG[3], J. VIEIRA[4] and W. B. MORI[1,3]

[1]Department of Electrical Engineering, University of California, Los Angeles, CA 90095, USA (mtzouf@ucla.edu)
[2]Los Alamos National Laboratory, Los Alamos, NM 87545, USA
[3]Department of Physics and Astronomy, University of California, Los Angeles, CA 90095, USA
[4]GoLP/Instituto de Plasmas e Fusão Nuclear, Instituto Superior Técnico, Technical University of Lisbon, Lisbon, Portugal

(Received 29 October 2011; accepted 26 January 2012; first published online 29 February 2012)

Abstract. Optimization of laser wakefield acceleration involves understanding and control of the laser evolution in tenuous plasmas, the response of the plasma medium, and its effect on the accelerating particles. We explore these phenomena in the weakly nonlinear regime, in which the laser power is similar to the critical power for self-focusing. Using Particle-In-Cell simulations with the code QuickPIC, we demonstrate that a laser pulse can remain focused in a plasma channel for hundreds of Rayleigh lengths and efficiently accelerate a high-quality electron beam to 100 GeV (25 GeV) in a single stage with average gradient 3.6 GV/m (7.2 GV/m).

1. Introduction

Electron acceleration in laser-driven plasma wakes results from the interplay of a number of nonlinear optical and plasma physics phenomena. Modifications to a given accelerator design can change the manifestation of one or more of these physical mechanisms with considerable effect on the final electron beam properties. Therefore, assessing the feasibility of a specific parameter choice requires good understanding of the physics and accurate simulations, even as most acceleration schemes that currently appear suitable for applications are underpinned by the same original idea of Tajima and Dawson (1979).

Much progress has been made in experiment, theory, and simulation of Laser WakeField Acceleration (LWFA) over the past 30 years, especially since electron beams with narrow energy spread were first observed in experiments by Faure et al. (2004), Geddes et al. (2004) and Mangles et al. (2004). Subsequently, quasi-monoenergetic electron beams have been consistently produced in experiments around the world, when intense ultra-short pulses have irradiated tenuous plasmas. However, the ability to predict the final properties of the accelerated electrons has been somewhat limited, because of the sensitivity of the physics to the experimental parameters. Recent experimental campaigns have concentrated not merely on reaching the highest possible electron energy but also on improving the shot-to-shot stability and on producing predictable and controllable behavior to facilitate the transition of LWFA from experiment to application.

Most of these experiments involve laser pulses that are intense enough to expel the plasma electrons from a near-spherical region. This bubble-like structure travels with velocity close to the speed of light and sustains strong accelerating and focusing fields, ideal for accelerating electrons. A phenomenological theory, based on 3D Particle-In-Cell (PIC) simulations, was developed by Lu et al. (2007) to provide a physical picture of the entire process and guide the choice of experimental parameters. This theory has been shown to be in good agreement with experiment, where the electron energies in current experiments are typically below 1 GeV.

In this paper we use reduced PIC simulations to confirm the scalings by Lu et al. (2007) for beams with energy up to 100 GeV. We show that the accelerator parameters can be scaled – even if non-trivially – from low- to high-energy accelerators while maintaining excellent quality. This is achieved in the weakly nonlinear regime, where the laser power is equal to the critical power for self-focusing $P \simeq P_c$. We investigate the suitability of the phenomenological theory in this weakly nonlinear regime and use the quasi-static PIC code QuickPIC (Huang et al., 2006) to model the physics up to these ultra-high energies.

In Sec. 2 we discuss the physics in the weakly nonlinear regime using 2-dimensional (2D) full-PIC simulations and simple analytical estimates. In Sec. 3 we briefly present some of the benchmarks for the QuickPIC simulations and the parameters for the high-energy simulations. The simulation results are shown in Sec. 4, and we summarize the conclusions from the theoretical and numerical calculations in Sec. 5.

https://doi.org/10.1017/S0022377812000232 Published online by Cambridge University Press

2. Acceleration in the weakly nonlinear regime

2.1. Efficiency

During the acceleration process, energy is continuously being transferred from the laser pulse to the plasma. The acceleration efficiency η can be defined as the ratio of the kinetic energy of the 'beam' electrons to the initial energy in the laser pulse, that is $\eta \equiv N\langle \Delta W_F\rangle/\mathscr{E}_L$, where $\langle \Delta W_F\rangle$ is the average final energy of the N beam electrons. The rest of the energy is partitioned between plasma electrons and electromagnetic fields, including unused energy in the laser pulse. In accordance, low efficiency indicates that most of the laser energy has been converted to heat in the plasma or it remains in the pulse. At these two extremes of low efficiency, one finds the ultra-relativistic regime, where the normalized vector potential $a_0 \equiv \frac{|e|A}{mc^2} \gg 1$, and the linear regime, where $a_0 \ll 1$. In the former, most of the laser energy is expended in increasing the kinetic energy of plasma electrons, while in the latter, the acceleration length is much shorter than the laser energy depletion length and most of the energy is still in the pulse at the end of the acceleration process.

2.1.1. Efficiency in the linear regime. In LWFA the injected electrons gain energy as long as they reside in the accelerating and focusing region of the wake, with the corresponding propagation distance known as 'dephasing length'. For low-intensity lasers ($a_0 \ll 1$), the dephasing length can be expressed as $L_{\phi,l} \simeq (\omega_0^2/\omega_p^2)\lambda_p/4$, where ω_0 is the laser frequency, $\omega_p = 4\pi n_p e^2/m$ the plasma frequency, and lowercase 'l' stands for 'linear'. On the other hand, the energy of such a laser pulse is depleted after a distance $L_{pd,l} \simeq (\omega_0^2/\omega_p^2)\lambda_p/a_0^2$ (Esarey et al., 1996), which means that only a fraction $L_{\phi,l}/L_{pd,l}$ of the laser energy is available during the acceleration process and the efficiency η_l is smaller than the ratio $L_{\phi,l}/L_{pd,l}$:

$$\eta_l < \frac{L_{\phi,l}}{L_{pd,l}} \simeq \frac{a_0^2}{4}, \qquad a_0 \ll 1. \tag{2.1}$$

As per (2.1), the efficiency increases for higher laser intensity and it becomes significant for $a_0 \to 2$, well beyond the range of validity of linear theory. For such intensities the ponderomotive force of the laser is strong enough to cause a density perturbation $\delta n/n_p > 1$ and the structure of the wake is inherently 3D.

2.1.2. Efficiency in the blowout regime. As the laser intensity increases (for $a_0 \gg 1$), a larger proportion of the laser energy is 'lost' to electrons that are shot forward by the laser's ponderomotive force (Decker et al., 1996). Thus, the laser energy depletion length (pump depletion length) becomes comparable to the dephasing length, i.e. the length after which the accelerating electrons outrun the wake, and the efficiency is mainly determined by the amount of energy in the plasma that is available to the electron beam via the accelerating structure.

Tzoufras et al. (2008, 2009) showed that the total accelerating force on an electron bunch with total charge Q_t, and charge profile optimized for some accelerating gradient E_t, is independent of that gradient and it is equal to $Q_t E_t = \frac{1}{4^3}(k_p R_b)^4 mc^2/r_e$, where R_b is the blowout radius and $r_e = e^2/(mc^2)$, the classical electron radius. If the bunch travels until it reaches the middle of the bubble, the average field it experiences is $\frac{1}{2}E_t$. The effective accelerating force becomes

$$\langle Q_t E_z\rangle = \frac{1}{2^7}(k_p R_b)^4 \frac{mc^2}{r_e}. \tag{2.2}$$

The acceleration length in the blowout regime is the dephasing length $L_\phi \simeq \frac{c}{c-v_\phi} R_b$, where v_ϕ is the phase velocity of the wake. Substituting $v_\phi = c[1 - C_\phi \omega_p^2/\omega_0^2]$, where C_ϕ is a constant, $0.5 < C_\phi < 1.5$, we obtain the acceleration length:

$$L_{acc} \simeq \frac{1}{C_\phi}\frac{\omega_0^2}{\omega_p^2} R_b. \tag{2.3}$$

The total energy absorbed by the bunch is

$$\mathscr{E}_b \simeq \langle Q_t E_z\rangle L_{acc} \simeq \frac{1}{2^7 C_\phi}\frac{\omega_0^2}{\omega_p^2}(k_p R_b)^5 \frac{mc^2}{k_p r_e}. \tag{2.4}$$

The energy in the laser pulse may be written as

$$\begin{aligned}\mathscr{E}_L &= \frac{\sqrt{\pi/\ln 2}}{2} P \tau_{FWHM} \simeq P \tau_{FWHM} \\ &= \frac{1}{2^4}\frac{\omega_0^2}{\omega_p^2}\frac{mc^2}{k_p r_e} a_0^2 w_0^2 \tau_{FWHM},\end{aligned} \tag{2.5}$$

where w_0 and τ_{FWHM} are the laser spot-size and pulse duration at full width half maximum, respectively. Substituting the prescription for a matched laser beam $c\tau_{FWHM} \simeq w_0 \simeq R_b \simeq 2\sqrt{a_0}/k_p$ (Lu et al., 2007) into (2.5) we obtain an expression for the efficiency η_b, where the subscript 'b' stands for 'blowout':

$$\eta_b \simeq \frac{\mathscr{E}_b}{\mathscr{E}_L} \simeq \frac{1}{2C_\phi}\frac{1}{a_0} \Rightarrow \frac{1}{3}\frac{1}{a_0} < \eta_b < \frac{1}{a_0}. \tag{2.6}$$

The lower bound shows the efficiency in the ultra-relativistic regime, where $a_0 \gg 1$ and the phase velocity of the wake is $v_\phi \simeq c[1 - 1.5\omega_p^2/\omega_0^2]$. The upper bound occurs for $a_0 \to 2$ and for a wake with phase velocity roughly equal to the linear group velocity of the laser $v_g \simeq c[1 - 0.5\omega_p^2/\omega_0^2]$ (see detailed discussion below). In both cases, the efficiency scales with the inverse laser strength parameter $\eta_b \propto a_0^{-1}$. Therefore, in the blowout regime the efficiency increases with the laser intensity, in contrast with the linear regime, where the efficiency scales as $\eta_l \propto a_0^2$. In other words, both linear and nonlinear theory suggest that LWFA is most efficient when $a_0 \simeq 2$.

2.2. Scaling formulas for lasers with power equal to the critical power for self-focusing

We apply the scaling formulas by Lu et al. (2007) for lasers with strength parameter $a_0 = 2$, for which clear

https://doi.org/10.1017/S0022377812000232 Published online by Cambridge University Press

blowout occurs. The condition for matched propagation is

$$k_p R_b \simeq k_p w_0 \simeq 2\sqrt{a_0} = 2\sqrt{2\left(\frac{P}{P_c}\right)^{1/3}}, \qquad (2.7)$$

where $P_c[GW] = 17\omega_0^2/\omega_p^2$ is the critical power for self-focusing. The pulse needs to fit in the first (decelerating) half of the plasma bubble, therefore

$$c\tau_{FWHM} \simeq R_b \simeq w_0. \qquad (2.8)$$

Assuming $a_0 = 2$, (2.7)–(2.8) yield:

$$P \simeq P_c, \qquad (2.9)$$

$$R_b \simeq c\tau_{FWHM} \simeq w_0 \simeq 2\sqrt{2}\frac{c}{\omega_p}. \qquad (2.10)$$

The energy of such a laser will be depleted after a distance:

$$L_{pd,b} \simeq 2\sqrt{2}\left(\frac{k_0^2}{k_p^2}\right)k_p^{-1}. \qquad (2.11)$$

Electrons placed at the back of the bubble will outrun the wake after

$$L_{\phi,b} \simeq \frac{4\sqrt{2}}{3}\left(\frac{k_0^2}{k_p^2}\right)k_p^{-1}. \qquad (2.12)$$

After traveling for a distance $L_{\phi,b}$, electrons in the bunch reach energy:

$$\langle \Delta W_b \rangle \simeq \frac{4}{3}\left(\frac{k_0^2}{k_p^2}\right)mc^2. \qquad (2.13)$$

The length of the beam σ_z scales with the size of the blowout radius, $\sigma_z \propto k_p^{-1}$, and the number of accelerating particles scales with the square root of the laser power, $N_b \propto \sqrt{P}$, (Pukhov and Gordienko, 2006; Lu et al., 2007). From (2.7)–(2.13) all of the laser parameters P, w_0, τ_{FWHM}, as well as the pump depletion and dephasing lengths, the energy gain $\langle \Delta W_b \rangle$, the length of the beam, and its charge can be expressed as a function of the plasma skin depth and the laser wavelength. Alternatively, for a given laser wavelength, using (2.9) all of the above quantities (including the plasma density) scale with some power of the laser power. These scalings are presented in Table 1. On the bottom of Table 1 we show the scaling of the QuickPIC simulation parameters, which will be discussed extensively later.

The formulas in the first column of Table 1 constitute an approximate description of LWFA in the blowout regime, where $a_0 \gg 1$, and need to be revisited for $a_0 \simeq 2$. Below we use quantities such as the distance $L_{\phi,b}$ from (2.12), even though this is not identical with the actual dephasing length in the weakly nonlinear regime. Besides, the dephasing length for externally injected electrons depends on the location of the injection. Notwithstanding the small discrepancy between the coefficients from the phenomenological theory by Lu et al. (2007) and those in the weakly nonlinear regime, the scalings themselves work remarkably well even for $a_0 \simeq 2$. To avoid confusion, we will use the formulas from the phenomenological theory for the blowout regime presented in this section and explain departures from these formulas when necessary.

Table 1. Scalings of the laser, plasma, and beam parameters with the laser power for fixed a_0 and λ_0. The scaling of the QuickPIC simulation parameters is also shown.

	Formulas (from Lu et al. (2007))	For fixed a_0, λ_0
Laser	$k_p w_0 = 2\sqrt{a_0}$ $c\tau_L = w_0$	$w_0 \propto \sqrt{P}$ $\tau_{FWHM} \propto \sqrt{P}$
Plasma	$a_0 = 2(P/P_c)^{1/3}$ $k_p R_b = 2\sqrt{a_0}$ $L_{\phi,b} = \frac{4}{3}\frac{k_0^2}{k_p^2}\frac{\sqrt{a_0}}{k_p}$	$n_p \propto P^{-1}$ $R_b \propto \sqrt{P}$ $L_{\phi,b} \propto P^{3/2}$
Beam	$\langle \Delta W_b \rangle = \frac{2}{3}mc^2\frac{k_0^2}{k_p^2}a_0$ $N_b = \frac{8/15}{k_0 r_e}\sqrt{\frac{P}{m^2c^5/e^2}}$ $\sigma_z \propto R_b$	$\langle \Delta W_b \rangle \propto P$ $N_b \propto \sqrt{P}$ $\sigma_z \propto \sqrt{P}$
Simulation	$\mathrm{Tmax} = k_p L_\phi$ $\#\mathrm{cells}_\perp \propto (k_p w_0)^2$ $\#\mathrm{cells}_z \propto \tau_{FWHM}$ $DT = \frac{1}{30}k_p Z_R$ Size $\propto$ (#cells) $\times\, \mathrm{Tmax}/DT$	$\mathrm{Tmax} \propto P$ $\#\mathrm{cells}_\perp = C$ $\#\mathrm{cells}_z \propto \sqrt{P}$ $DT \propto \sqrt{P}$ Size $\propto P$

2.3. Frequency shifts

2.3.1. Laser guiding with a density channel in the blowout regime. In the nonlinear regime, using the matching condition to avoid violent oscillations of the transverse laser profile is only meaningful if the preconditions for the pulse to remain guided are satisfied. In the linear regime, a parabolic plasma density channel with profile $n = n_p + \Delta n_c r^2/w_0^2$, where $\Delta n_c = \frac{1}{\pi r_e w_0^2} = \frac{4}{(k_p w_0)^2}n_p$ can provide the necessary modification to the refractive index to guide a Gaussian laser pulse with spot-size w_0 (Esarey et al., 1997). Therefore, for pulses with $P \simeq P_c$, where the etching mechanism does not dominate (see below) and self-guiding is not sufficient to ensure stable laser propagation, we combine a parabolic density channel with the matching condition (2.7) to obtain

$$\frac{\Delta n_c}{n_p} \simeq \frac{1}{a_0}, \qquad (2.14)$$

and for $a_0 \simeq 2 \Rightarrow \frac{\Delta n_c}{n_p} \simeq \frac{1}{2}$. This parabolic density channel with depth evaluated from (2.14) guides the front of the laser while the main body of the pulse remains guided due to the ponderomotive blowout.

2.4. Evolution of the spectral content of the laser

2.4.1. Photon deceleration in PIC simulations. In the blowout regime, the energy of the laser pulse is depleted due to the interaction of its leading edge with an electron density spike, which moves with the same speed as the rest of the accelerating structure. Over time, the front of the laser etches back until the pulse runs out of energy (Decker et al., 1996). This process is associated with the deceleration of laser photons.

Photon deceleration can be visualized with the help of the Wigner transform, which for a function $\varphi(z)$ is

https://doi.org/10.1017/S0022377812000232 Published online by Cambridge University Press

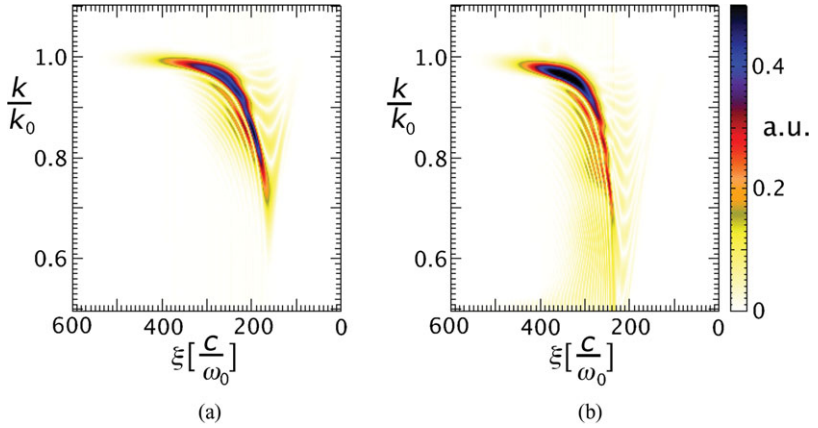


Figure 1. (Colour online) The profile of the spectral content of an ultra-intense pulse is characterized by rapidly decelerating photons at the leading edge, while the photons in the main body of the pulse travel with constant momentum. (The pulse travels from left to right.) The Wigner transform of the ξ-axis ($\xi = ct - z$) lineout of the laser field, for a pulse with $a_0 = 6$, is shown after a propagation distance (a) $c\tau \simeq 2.9\,\mathrm{cm} \simeq L_{\phi,b}/4$, and (b) $c\tau \simeq 5.8\mathrm{cm} \simeq L_{\phi,b}/2$.

defined as $W_\varphi(z,k) \equiv \int_{-\infty}^{\infty} e^{-ikz'} \varphi(z + \frac{z'}{2}) \varphi^*(z - \frac{z'}{2}) dz'$. In Fig. 1 we present the Wigner transform of the laser electric field along the propagation axis (ξ-axis) of a 2-PW pulse from a 2D simulation performed with the PIC code OSIRIS (Fonseca et al., 2002, 2008). The pulse has a rise-time $\tau_r = 80\,\mathrm{fs}$, fall-time $\tau_f = 190\,\mathrm{fs}$, spot-size $w_0 = 41\,\mu\mathrm{m}$, and $a_0 = 6$, which for a laser with wavelength $\lambda_0 = 0.8\,\mu\mathrm{m}$ corresponds to power $P \simeq 2\,\mathrm{PW}$. The laser parameters are matched for a uniform plasma with density $n_p \simeq 4 \times 10^{17}\mathrm{cm}^{-3}$. A moving window with dimensions $800 \times 8000 \frac{c}{\omega_0}$ was resolved by a grid with 4000×512 cells, four particles per cell were used, and the simulation ran for 5×10^6 time-steps with $\Delta t = 0.19972\omega_0^{-1}$.

In this ultra-relativistic regime the Wigner transform of the laser develops the 'hockey stick' shape shown in Fig. 1 soon after the acceleration process has started. As the front of the laser excites the wake, its wavenumber drops by $\Delta k_0 = k - k_0$. The energy of the laser photons in the front of the pulse also decreases $\frac{\Delta\omega_0}{\omega_0} \simeq \frac{\Delta k_0}{k_0}$ and it is transferred to plasma electrons. Meanwhile, the photons in the main body of the pulse propagate in vacuum with momentum $k \simeq k_0$. The Wigner transform of the laser pulse exhibits a similar shape at all subsequent times with a region of sharply decelerating photons in the front and a shortening body of photons with $k \simeq k_0$ in the back. When the supply of fresh photons with $k \simeq k_0$ runs out, the energy of the pulse is depleted.

In the linear regime, the observed shape of the Wigner transform resembles a 'check mark' with the rate of deceleration exhibiting a maximum near the back of the pulse (Gordon et al., 2003). The case with $P/P_c \simeq 1 \Rightarrow a_0 \simeq 2$ studied in this paper lies in between the ultra-relativistic blowout regime in Fig. 1 and the linear regime discussed by Gordon et al. (2003). For $a_0 \simeq 2$ blowout does occur, and the back of the pulse can be expected to remain in vacuum with $k \simeq k_0$; however, the length of the interaction region between the laser and the plasma is comparable to the pulse length such that a significant portion of the laser red-shifts, not just the leading edge.

Table 2. Laser parameters and plasma density for three 2D simulations with OSIRIS. The laser vector potential is $a_0 = 2$ for all three runs and guiding was achieved with the use of a plasma channel with width matched to w_0 as in (2.14).

P (TW)	τ(fs)	$w_0(\mu\mathrm{m})$	$n_p(10^{18}\mathrm{cm}^{-3})$
15	36	11	2
30	50	15	1
60	71	22	0.5

We performed 2D PIC simulations for three lasers (see Table 2) with matched parameters such that $a_0 \simeq 2$. The Wigner transforms of the ξ-axis laser field are presented in Fig. 2. Each row corresponds to one simulation and the Wigner transform is shown after a propagation distance is expressed as a fraction of $L_{\phi,b}$. This figure indicates that the propagation distance $c\Delta\tau$ required for a certain percentage of photon deceleration $\frac{\Delta k_0}{k_0}$ to take place is proportional to $L_{\phi,b}$. This simulation result can be written as

$$c\Delta\tau \simeq f(a_0)\frac{\Delta k_0}{k_0} L_\phi,$$

where f is some function of a_0. This expression is corroborated by the analytical calculation in the following section. The shape of the Wigner transform is indeed a combination of the 'check sign' observed in the linear regime (Gordon et al., 2003) and the shape shown in Fig. 1.

2.4.2. Scaling of photon deceleration with propagation distance. To derive an expression for the frequency shift as a function of the distance ξ from the front of the pulse we start from the 1D quasistatic expression for the plasma response ψ (Sprangle et al., 1990):

$$\frac{\partial^2\psi}{\partial\xi^2} - \frac{k_p^2}{2}\left[\frac{1+a^2}{(1+\psi)^2} - 1\right] = 0,$$

https://doi.org/10.1017/S0022377812000232 Published online by Cambridge University Press

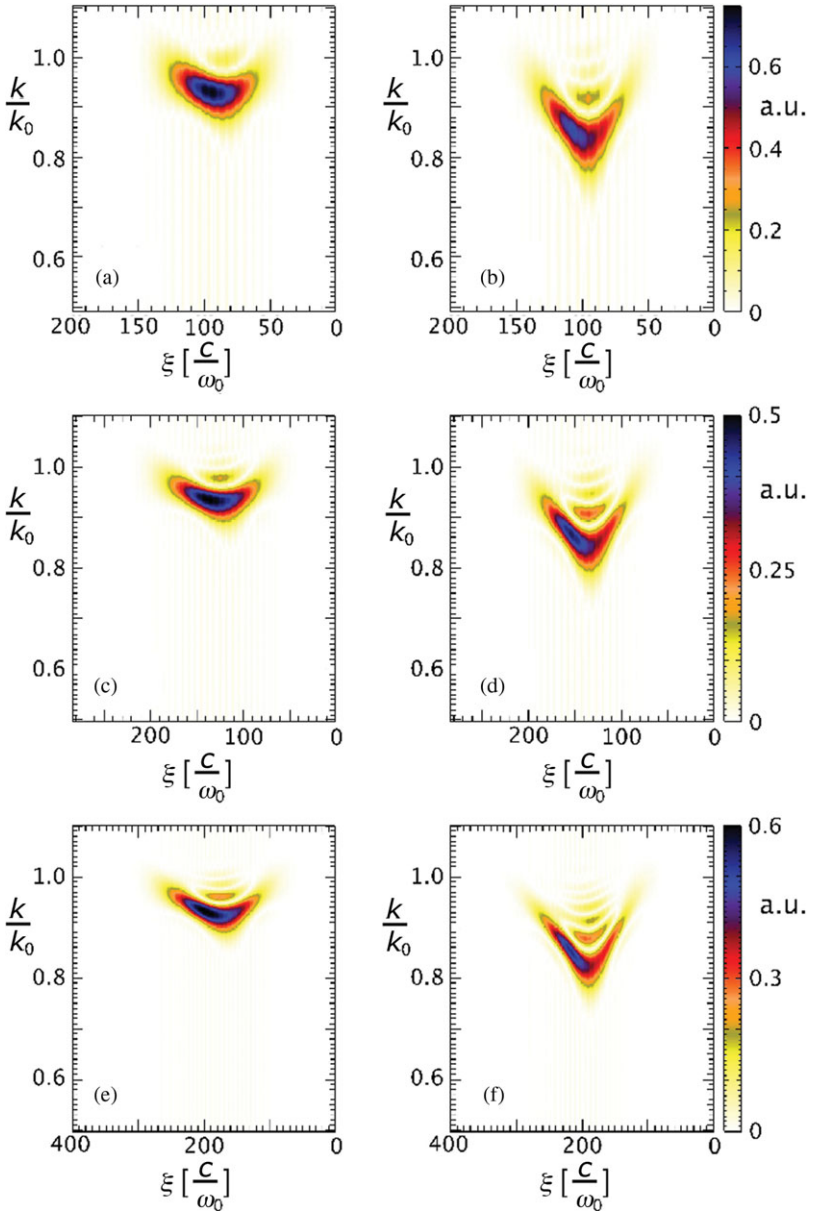


Figure 2. (Colour online) The spectral content of a laser in the weakly nonlinear regime ($a_0 = 2$) evolves in a way that has similarities with both linear $a_0 \ll 1$ and nonlinear $a_0 \gg 1$ regimes. Furthermore, it looks the same at a specified fraction of $L_{\phi,b}$ irrespective of the laser power (for a properly matched pulse). The Wigner transforms of the ξ-axis lineout of the laser field for pulses with $a_0 = 2$ are shown after a propagation distances $c\tau \simeq L_{\phi,b}/4$ [(a), (c), and (e)] and $c\tau \simeq L_{\phi,b}/2$ [(b), (d), and (f)]. Plots (a) and (b) correspond to a 15-TW laser propagating in $2 \times 10^{18}\mathrm{cm}^{-3}$; plots (c) and (d) to 30 TW and $1 \times 10^{18}\mathrm{cm}^{-3}$, and plots (e) and (f) to 60 TW and $5 \times 10^{17}\mathrm{cm}^{-3}$.

where $\xi = ct - z, \tau = t$ are the speed of light coordinates and we assume that $|\boldsymbol{a}|$ is a square-shaped pulse $|\boldsymbol{a}| = a_0 \int_{-\infty}^{\xi} d\xi[\delta(\xi) - \delta(\xi - c\tau_L)]$. For $0 < \xi < c\tau_L, a_0 = \text{const}$, there is translational symmetry in ξ and we can substitute $\psi'' \to \psi' \frac{\partial \psi'}{\partial \psi}$ (where prime denotes differentiation with respect to ξ) and integrate

$$\left(\frac{\partial \psi}{\partial \xi}\right)^2 = -k_p^2\left[\frac{1+a_0^2}{1+\psi} + \psi\right] + C.$$

In the quasi-static approximation, the wakefield is $E_\parallel = \frac{\partial \psi}{\partial \xi}$. Since $E_\parallel = 0$ in front of the pulse, $\frac{\partial \psi}{\partial \xi}|_{\xi=0} = 0 \Rightarrow C = k_p^2(1 + a_0^2)$. Substituting this expression for C into the above equation yields

$$\frac{\partial \psi}{\partial \xi} = k_p \sqrt{\frac{\psi}{1+\psi}|a_0^2 - \psi|}. \tag{2.15}$$

This equation can be solved for $\xi(\psi)$ and the solution is a function of elliptic integrals.

In the context of the quasi-static approximation, the index of refraction takes the form:

$$\eta \simeq 1 - \frac{1}{2}\frac{k_p^2}{k^2}\frac{1}{1+\psi}.$$

Changes in the index of refraction modify the local wavenumber of the laser pulse due to photon

https://doi.org/10.1017/S0022377812000232 Published online by Cambridge University Press

acceleration/deceleration (Mori, 1997):

$$\frac{1}{k}\frac{\partial k}{\partial(c\tau)} = -\frac{1}{\eta^2}\frac{\partial \eta}{\partial \xi}. \tag{2.16}$$

Under the assumption that the laser spectral content is a weaker function of ξ than the plasma response ψ, and more specifically for $\frac{3}{k}\frac{\partial k}{\partial \xi} \ll \frac{1}{1+\psi}\frac{\partial \psi}{\partial \xi}$, we obtain

$$\frac{1}{k}\frac{\partial k}{\partial(c\tau)} \simeq -\frac{1}{2}\frac{k_p^2}{k^2}\frac{1}{(1+\psi)^2}\frac{\partial \psi}{\partial \xi}. \tag{2.17}$$

Assuming that the pulse is square-shaped, $|\boldsymbol{a}| = a_0 \int_{-\infty}^{\xi} d\xi[\delta(\xi) - \delta(\xi - c\tau_L)]$ and substituting (2.15) into (2.17) we obtain

$$\frac{1}{k}\frac{\partial k}{\partial(c\tau)} \simeq -\frac{1}{2}\frac{k_p^3}{k^2}\frac{\sqrt{\psi(a_0^2-\psi)}}{(1+\psi)^{5/2}}. \tag{2.18}$$

This expression for $\frac{1}{k}\frac{\partial k}{\partial(c\tau)}$ exhibits a maximum (at ψ_+):

$$\begin{aligned}\psi_+ &\simeq \frac{1}{3}(1+2a_0^2-\sqrt{1+a_0^2+4a_0^4}) \\ &\simeq \frac{1}{4}-\frac{1}{12a_0^2}, \text{ for } a_0 \gg 1.\end{aligned} \tag{2.19}$$

The maximum rate of change of the wavelength for $a_0^2 \gg 1$ occurs at a fixed location behind the front of the pulse: $\psi \simeq 1/4 \ll 1 \Rightarrow \xi \simeq (k_p a_0)^{-1} \equiv \xi_{dm}$. At $\xi = \xi_{dm}$, the rate of photon deceleration is

$$\left.\frac{1}{k}\frac{\partial k}{\partial(c\tau)}\right|_{\max} \simeq \left.\frac{1}{k}\frac{\partial k}{\partial(c\tau)}\right|_{k_p\xi \simeq a_0^{-1}} \simeq -0.143\frac{k_p^3}{k^2}a_0. \tag{2.20}$$

Using (2.20) we can estimate the distance $c\Delta\tau$ that the laser travels until the change in its original wavenumber becomes

$$\frac{\Delta k_0}{k_0} \simeq -0.11 a_0^{3/2}\frac{c\Delta\tau}{L_{\phi,b}}. \tag{2.21}$$

From (2.21) we see that for lasers with fixed intensity the propagation distance required to reach a specific level of photon deceleration $\Delta k_0/k_0$ scales in the same way as the dephasing length, and that significant photon deceleration occurs earlier/later in the acceleration process when the laser intensity is increased/reduced.

Equations (2.17)–(2.21) are strictly valid when $\frac{3}{k}\frac{\partial k}{\partial \xi} \ll \frac{1}{1+\psi}\frac{\partial \psi}{\partial \xi}$. For low a_0, $a_0 \sim 2$, such as in the simulations presented in this paper, this can be true up to a propagation distance comparable to $L_{\phi,b}$. For $a_0 > 2$ this approximation holds at the early stages of the acceleration process, before the Wigner transform of the laser field starts resembling the 'hockey stick' shape discussed earlier, at which point k is very localized (in ξ) and the etching mechanism dominates.

2.4.3. Phase velocity of the wake. The spectral behavior of the laser directly impacts the phase velocity of the wake. For a laser with strength parameter $a_0 \gg 1$ only photons at the leading edge of the pulse interact with the plasma and their energy quickly drops as they decelerate. As a result of this mechanism the phase velocity of the wake becomes $\frac{v_{\phi,a_0\gg1}}{c} \simeq 1 - \frac{3}{2}\frac{\omega_p^2}{\omega_0^2}$.

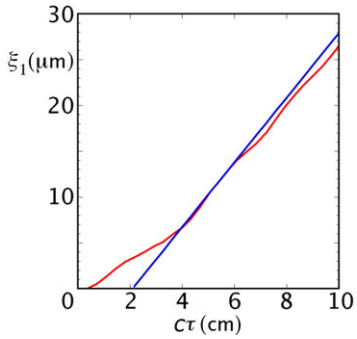


Figure 3. (Colour online) For ultra-intense lasers, after a transient time the laser evolution is dominated by local depletion of the leading edge of the pulse (etching mechanism). In this figure we show the location ξ_1 where $\psi = 1$ as a function of the propagation distance of the laser pulse for a 2-PW laser matched so that $a_0 \simeq 6$. The red line corresponds to the measurement from the 2D OSIRIS simulation and the blue line is drawn assuming an etching velocity as $v_{\text{etch}} = \frac{3}{2}\frac{\omega_p^2}{\omega_0^2}$.

To confirm this, we measured v_ϕ from the 2D PIC simulation for a 2-PW laser described earlier (see Fig. 1). In Fig. 3 we plot the location ξ_1 where $\psi(\xi_1) = 1$ for this simulation (red curve) over the propagation distance $c\tau$ and compare it with a line (blue line) with slope that corresponds to the phase velocity expected from the etching mechanism. It can be observed that after a transient time, during which the laser self-steepens (Vieira et al., 2010) and its spectral content is being transformed to the "hockey stick" shape shown in Fig. 1, the phase velocity settles to the value predicted by theory. From this point on, the phase velocity (slope of the red curve), as shown in Fig. 3, does not change much.

For $a_0 = 2$ the entire pulse red-shifts with a rate that depends on the exact location of the photons. This means that the etching mechanism does not dominate the laser evolution, at least not until the last stages of the acceleration process. However, we cannot use the formula for the linear group velocity $\frac{v_{g,l}}{c} = 1 - \frac{1}{2}\frac{\omega_p^2}{\omega_0^2}$ either, because in this regime the laser frequency is an unknown function of both ξ and τ. In Fig. 4 we plot the location ξ_1 as a function of the propagation distance $c\tau$ for the simulations described in Table 2. In each of these plots the red curve is the measurement from the simulation and the green line corresponds to the linear group velocity of the laser. From Fig. 4 we notice that even though the changes in the local frequency can be significant, for distances up to $L_{\phi,b}$ the linear group velocity approximates the simulation result well. Near the end of the simulation, as the frequency drops further, the group velocity of the laser decreases and energy depletion becomes more localized. At that stage the slope of the simulation curve in Fig. 4 increases (and the red simulation curve intersects the green line) and may be better approximated by using the etching mechanism. Despite the intricacies of the evolution of

https://doi.org/10.1017/S0022377812000232 Published online by Cambridge University Press

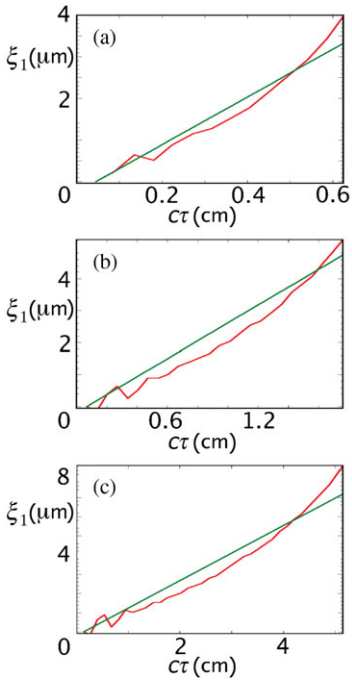


Figure 4. (Colour online) For weakly nonlinear pulses ($a_0 \simeq 2$) the linear group velocity is a good approximation early in the acceleration process, but the etching mechanism is more appropriate at the end. We show the location ξ_1 where $\psi = 1$ as a function of the propagation distance of the laser pulse for the three runs in Table 2. The red line corresponds to the measurement from the 2D OSIRIS simulations and the green line is drawn assuming the linear group velocity of the laser $\frac{v_{g,l}}{c} = 1 - \frac{1}{2}\frac{\omega_p^2}{\omega_0^2}$. (a) A 15-TW laser, (b) a 30-TW laser, and (c) a 60-TW laser.

the spectral content, Fig. 4 indicates that the scalings in Table 1 are valid in the weakly nonlinear regime.

2.5. Beam loading

In the blowout regime, particles can be self-injected at the rear of the bubble and load the accelerating phase of the wake. In order to limit the energy spread and utilize the wake in the most efficient manner, methods that allow for controlled injection of particles are being investigated (Faure et al., 2006; Pak et al., 2010; Kalmykov et al., 2011; Pollock et al., 2011; Vieira et al., 2011). An analytical theory for beam loading in the blowout regime ($a_0 \gg 1$) was also recently developed (Tzoufras et al., 2008, 2009). The analytical expressions in this theory employed the assumption that the width of the plasma sheath around the ion channel can be ignored compared to radius of the channel. For $a_0 = 2$ this assumption is inaccurate at the rear of the bubble, which is where the externally injected particles are loaded.

An exact solution for beam loading in this regime ($a_0 = 2$) can be obtained by numerically solving for the shape of the bubble. Here we are interested in the scaling of the formulas rather than their exact form. These scalings are the same as in the case $a_0 \gg 1$, that is, the length of the bunch and the total charge scale with the square root of the laser power. In addition, since properly loaded Gaussian bunches can lead to nearly constant accelerating field within the bunch (Tzoufras et al., 2008, 2009), these may be used to achieve low-energy spread. Finally, the energy spread of the electron beam depends on the effect of beam loading on all different phases of the wake. It was argued by Tzoufras et al. (2009) and Rechatin et al. (2010), and it will be shown here from the simulations that such beams maintain low-energy spread throughout the acceleration process.

2.6. Radiation

The effect of the reaction force due to synchrotron radiation can be calculated by substituting the equations for the unperturbed electron orbits (Michel et al., 2006) into the classical expression. Lu et al. (2007) derived an estimate for the beam spot-size $\sigma_{r,0.01}$ for which the ratio of the loss of energy due to synchrotron radiation to the energy gain is $\frac{\Delta\gamma}{\gamma} \leqslant 0.01$. Using the scaling laws for $a_0 = 2$ to rewrite the beam energy and plasma density in terms of the laser power we obtain

$$\sigma_{r,0.01}[\mu m] \leqslant \frac{47.7}{(P[TW])^{1/4}}. \tag{2.22}$$

We reiterate that (2.22) assumes that all of the laser and plasma parameters have been chosen according to the formulas for the blowout regime.

3. Setup of the QuickPIC simulations

Three-dimensional PIC codes have been successfully compared with LWFA experiments (Tsung et al., 2006) and used to confirm scaling formulas, but the computational requirements of these codes prevent simulating LWFA with gain exceeding 10 GeV for lasers with $a_0 < 6$. Moreover, what is required to optimize laser wakefield accelerators is not merely isolated simulations, but parameter scans with detailed diagnostics. Quasi-static PIC codes offer the ability to carry out such simulations. We note that since the work in this paper was first performed (Tzoufras, 2008), simulations of LWFA using a full-PIC code in a boosted frame have been carried out for related parameters (Martins et al., 2010).

3.1. Benchmarking of QuickPIC

QuickPIC is a numerical code developed specifically for plasma and laser wakefield accelerators (Huang et al., 2006). It employs the envelope approximation for the laser and the quasi-static approximation for the plasma electrons (Mora and Antonsen 1997; Huang et al. 2006; Lu et al. 2006 a, b).

The quasistatic approximation assumes that the driver remains unchanged in the time it takes to pass by a plasma electron. This implies that there are no trapped particles in the system other than those treated as beams, which are incorporated separately. Here we will present results from simulations with $a_0 = 2$, which is

https://doi.org/10.1017/S0022377812000232 Published online by Cambridge University Press

too low to ponderomotively generate fast electrons that travel in front of the pulse. In the back of the bubble, self-injection is suppressed, because the wake is loaded (externally) almost to capacity, and because a_0 is small to begin with.

3.2. Photon deceleration in QuickPIC

Since QuickPIC uses the laser envelope instead of the full laser field, we need to find the minimum spatial resolution that captures the laser spectral evolution properly for a distance equal to $L_{\phi,b}$. Setting $k_0\Delta z = \text{const}$, we found that the envelope description works well until a specific level of photon deceleration $\Delta k_0/k_0$ is reached. Therefore, for a given resolution $k_0\Delta z$, QuickPIC models the behavior of the laser well up to a distance that scales as $L_{\phi,b} \simeq \frac{4}{3}\frac{k_0^2}{k_p^2}\frac{\sqrt{a_0}}{k_p}$. From 2D OSIRIS simulations we found that for $a_0 \simeq 2$ the laser propagates for a distance equal to $L_{\phi,b}$ before $\Delta k_0/k_0 \simeq -0.5$. This result is in good agreement with (2.21) when $c\Delta\tau = L_{\phi,b}$ is used. We followed the evolution of the laser in QuickPIC, using $k_0\Delta z = 2.45$, for the same parameters as in the OSIRIS simulations, for the three cases described in Table 2. In all three cases the laser envelope in QuickPIC was in excellent agreement with the laser field in 2D OSIRIS until $L_{\phi,b}$ was reached.

3.3. Beam loading with QuickPIC

To confirm that an externally injected electron bunch will feel the same accelerating force in QuickPIC as it would in 3D OSIRIS, we compared a QuickPIC and a 3D OSIRIS simulation for the parameters in the first row of Table 2 (the importance of using 3D simulations as opposed to 2D was discussed by Vieira *et al.* 2008). In QuickPIC the simulation window has a size $40 \times 176 \times 176\ \mu m$ and is resolved by $2^7 \times 2^7 \times 2^7$ cells. The simulation ran for 450 time-steps with $\Delta T = 4\omega_p^{-1}$. In the OSIRIS simulation we used a grid with $1500 \times 160 \times 160$ cells to resolve a moving window with dimensions $300 \times 640 \times 640\ \frac{c}{\omega_0}$ (which corresponds to resolutions $k_0\Delta z = 0.2, k_p\Delta x = k_p\Delta y \simeq 0.14$). The resulting accelerating field E_z from the two codes is plotted in Fig. 5 at three different instants in time.

The location where the electron bunch resides can be recognized by its effect on the wake. The main body of the electron bunch causes the wake (E_z) to flatten. After the bunch the wakefield from OSIRIS (blue line) decreases rapidly, while that from QuickPIC (orange line) remains relatively flat. The wakefield experienced by the bunch is almost identical for the two simulations. This is corroborated by the energy distribution in Fig. 6. The red line corresponds to the energy distribution of the externally injected electron bunch from the 3D OSIRIS simulation and the blue line corresponds to the one from QuickPIC. The average energy gain for the two cases (OSIRIS and QuickPIC) is very close. We conclude that the wakefield from 3D OSIRIS and QuickPIC has the same effect on an externally injected electron bunch and

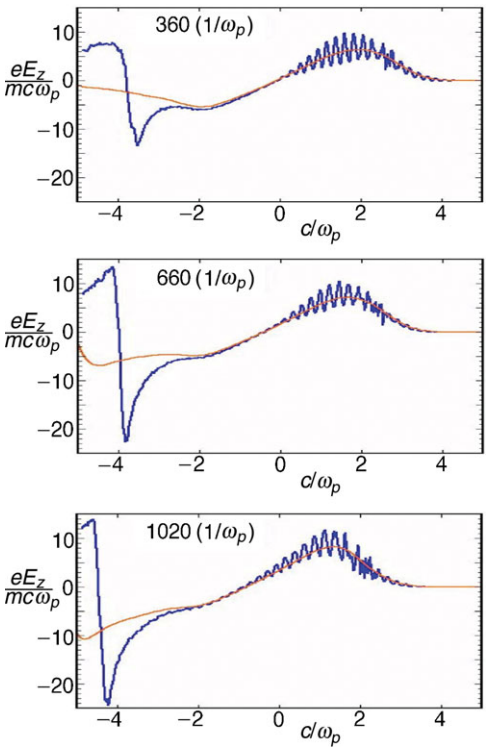


Figure 5. (Colour online) Three plots correspond to three instants in time from a simulation with 3D OSIRIS and a simulation with QuickPIC using the same parameters. The wakefield from the 3D OSIRIS (QuickPIC) simulation is drawn with the blue (orange) line. These plots show that throughout the acceleration process, the field experienced by the electron bunch is almost identical for the two codes.

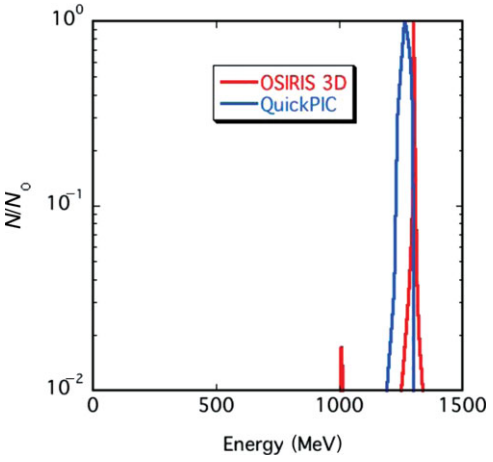


Figure 6. (Colour online) The red/blue line corresponds to the energy distribution of the externally injected electron bunch from the 3D OSIRIS/QuickPIC simulation. The average energy gain for the two cases is very close.

that by using QuickPIC we will obtain results similar to those one would expect from a 3D full-PIC simulation.

3.4. Simulation parameters with QuickPIC

QuickPIC allows us to access accelerator designs beyond what can be typically simulated with full-PIC codes. Here we investigate the regime $P \simeq P_c$ for which the scalings were described in Table 1. Following these

https://doi.org/10.1017/S0022377812000232 Published online by Cambridge University Press

Table 3. Accelerator designs for $P \simeq P_c$ and $\lambda_0 = 0.8\,\mu$m derived from the scalings in Table 1. For these parameters a plasma channel with depth $\frac{\Delta n_c}{n_p} \simeq \frac{1}{2}$ is required for guiding the laser pulse.

$\frac{\langle \Delta W \rangle}{\text{GeV}}$	$\frac{P}{\text{TW}}$	$\frac{\tau}{\text{fs}}$	$\frac{w_0}{\mu\text{ m}}$	$\frac{n_p}{\text{cm}^{-3}}$	$\frac{L_\phi}{\text{m}}$	$\frac{\langle E_z \rangle}{\text{GeV/m}}$	$\frac{\sigma_z}{\mu\text{m}}$	$\frac{N}{10^{10}}$
0.4	15	35.6	10.68	2E+18	0.0068	59.08	1.5	0.05
1.6	60	71.2	21.36	5E+17	0.0542	29.54	3	0.1
6.4	240	142.4	42.72	1.25E+17	0.4333	14.77	6	0.2
25.6	960	284.8	85.44	3.13E+16	3.4663	7.385	12	0.4
102.4	3840	569.6	170.9	7.81E+15	27.731	3.693	24	0.8
409.6	15360	1139.2	341.8	1.95E+15	221.84	1.846	48	1.6
1638.4	61440	2278.4	683.5	4.88E+14	1774.8	0.923	96	3.2

scalings, we obtain the accelerator designs presented in Table 3.

The main restriction in the QuickPIC simulations is the condition $k_0\Delta z \leqslant 2.45$ described earlier as a result of which $2^7 \times \sqrt{P(\text{TW})/15}$ cells must be used in the direction of the laser propagation. Each transverse slice contains $2^7 \times 2^7$ cells and the size of the moving window is $10.6 \times 46.8 \times 46.8\,\frac{c}{\omega_p}$ for all of the QuickPIC simulations. To accurately model the laser evolution, the 3D time-step of the simulation needs to be short enough to resolve the characteristic time of the laser envelope dynamics, which is the time it takes for the pulse to travel one Rayleigh length $Z_R = \frac{1}{2}k_0 w_0^2$. Therefore, we take $c\Delta T \simeq Z_R/30$ and the simulations in Table 3 require $450 \times \sqrt{P(\text{TW})/15}$ time-steps. For the simulation in the first (fifth) row of Table 3 the number of 3D time-steps is a factor of 10^3 (10^5) smaller than that for an OSIRIS simulation.

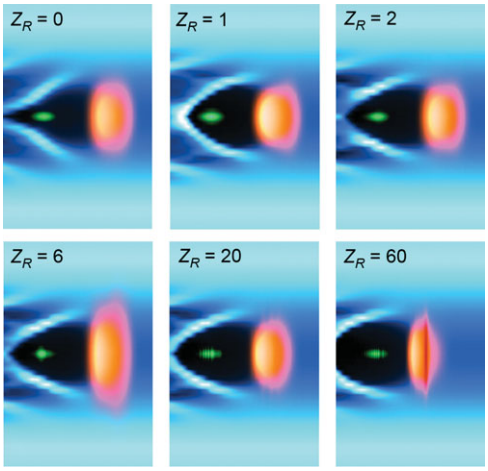


Figure 7. (Colour online) Six snapshots (zoomed in the transverse direction) from the simulation corresponding to the third row of Table 3 (6.4 GeV, 240 TW). The plasma density is in blue, the density of the electron beam is in green at the rear of the plasma bubble, and the laser intensity is in orange. The pulse propagates for $60\,Z_R$.

4. Simulation results

In designing the simulations for $P = P_c$ we assumed that the laser propagates in the plasma channel for a distance that can be arbitrarily long. Since the Rayleigh length scales with the laser power $Z_R = k_0 w_0^2/2 \propto P$ and the acceleration distance scales as $P^{3/2}$, it is clear that as we increase the laser power we expect the laser to remain focused for an increasing number of Rayleigh lengths. In Fig. 7 we present the plasma density in blue, the density of the externally injected electron beam in green (see the bunch at the rear of the plasma bubble), and the laser intensity in orange for the accelerator design in the third row of Table 3. The front of the laser is guided in the plasma channel and the back in the ponderomotively blown-out region. For this 6.4-GeV accelerator the length of the plasma channel is 0.43 m and it corresponds to $60\,Z_R$. The acceleration process shown in Fig. 7 is very stable, with a bubble of nearly constant radius throughout. An externally injected electron bunch starts at the back of the bubble and ends up near the middle after $60\,Z_R$.

The lineout of the wakefield (E_z) after $L_{\phi,b}/3$, $2L_{\phi,b}/3$, and $L_{\phi,b}$ is presented in Fig. 8 with a red line. The location where the bunch is loaded is shown with vertical broken lines. In the same figure we show the wakefield from the runs in the first and second rows of Table 3 with blue and green lines, respectively. The corresponding propagation lengths, which can be found in Table 3, in terms of the Rayleigh lengths are: $15\,Z_R$ for the 0.4 GeV/15 TW case and $30\,Z_R$ for the 1.6 GeV/60 TW case. The axes for all three plots in Fig. 8 are normalized such that if the scaling formulas (Lu et al., 2007) hold exactly, all lines should fall on top of each other.

It is clear that as we use higher powers and longer propagation lengths, the average wake appears to be weaker in these normalized units. This weakening of the accelerating field can be attributed to the fact that the laser needs to propagate for an increasing number of Z_R, and even if we assume that a very small percentage of its energy is lost to diffraction in each Rayleigh length, this loss will accumulate over the entire acceleration process. This effect could be easily compensated for by slightly adjusting the accelerator parameters, such as the charge of the bunch, the laser power, etc.

The energy distributions for the parameters in Table 2 are presented in Fig. 9. The purple and the light-blue lines also correspond to the first two rows from Table 3. It can be seen from the energy distribution that the

https://doi.org/10.1017/S0022377812000232 Published online by Cambridge University Press

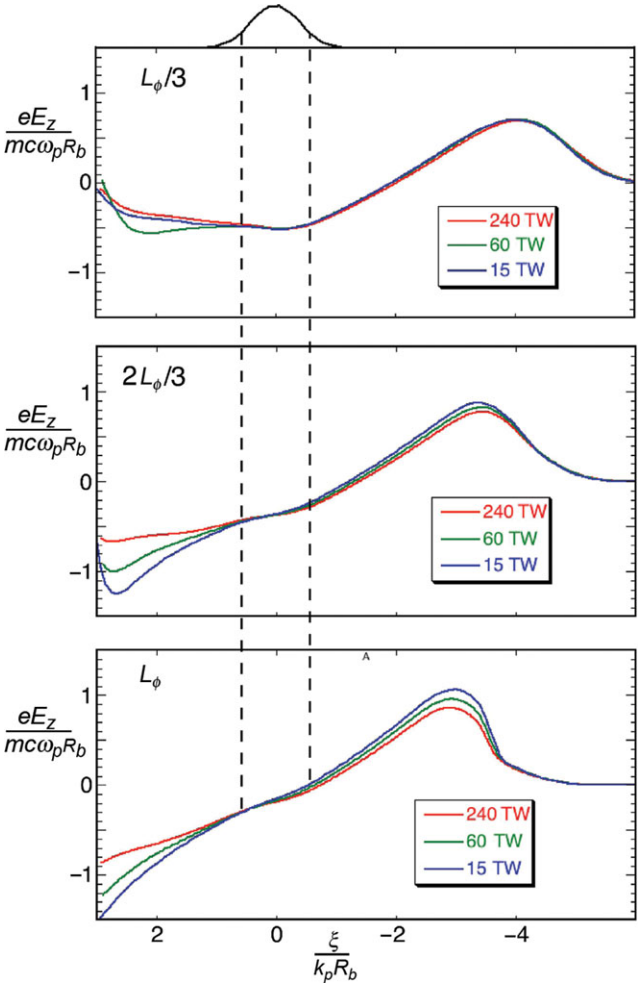


Figure 8. (Colour online) The wakefield E_z after $L_{\phi,b}/3$, $2L_{\phi,b}/3$, and $L_{\phi,b}$ for the three accelerator designs in the first three rows of Table 3.

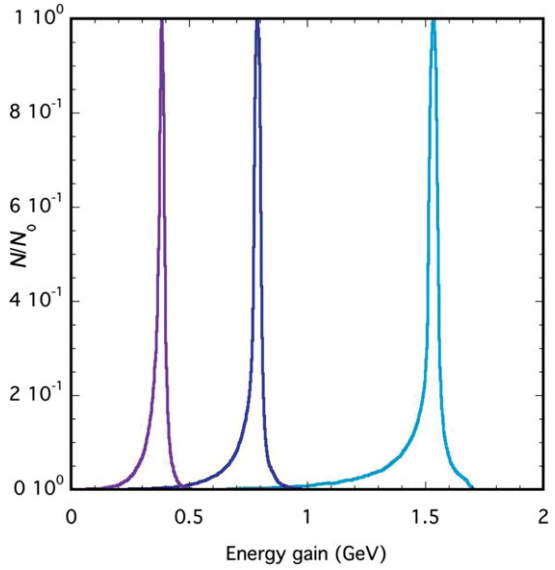


Figure 9. (Colour online) Energy distribution for the three simulations in Table 2.

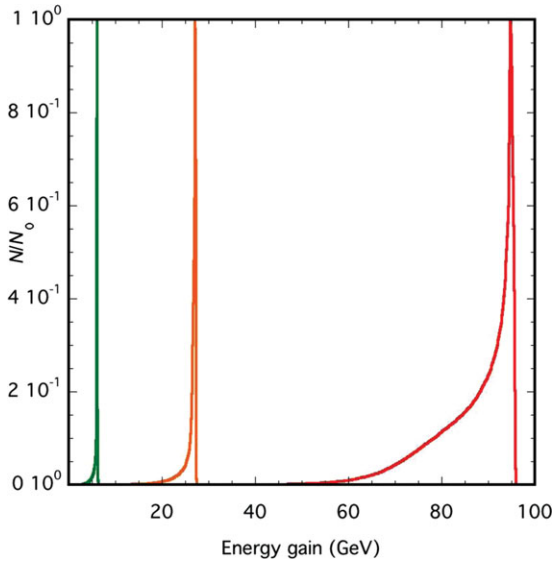


Figure 10. (Colour online) Energy distribution for the accelerator designs in the third, forth, and fifth row in Table 3. Only 2.458×10^9 electrons were loaded in the case of the 960 TW design and only 3.932×10^9 electrons were loaded for the 3.84 PW design. The peaks in the energy distribution are at 6.1 GeV, 27.1 GeV, and 94.9 GeV, and the corresponding energy spreads at full width half maximum are 0.5 GeV, 0.4 GeV, and 1.6 GeV.

scaling for the energy gain works excellently. The energy spread is also similar in all cases.

Since the normalized wake becomes weaker as we move to accelerator designs for higher energies, only 2.458×10^9 (instead of 4×10^9) electrons were loaded in the wake of the 960-TW laser shown in Table 3, and only 3.932×10^9 (instead of 8×10^9) for the 3.84-PW laser. For the accelerator designs in the third, fourth, and fifth rows of Table 3, the QuickPIC simulations yield the energy distributions shown in Fig. 10. The energy scaling works well, with the measured peaks of the energy distribution at 6.1 GeV, 27 GeV, and 95 GeV for these three simulations. The slightly higher-than-expected energy, as well as the improvement in the energy spread observed in the simulation for the 960-TW design, is due to the fact that the number of electrons was significantly smaller than what was predicted from the scalings. For the 3.84-PW simulation the laser was depleted of its energy before reaching the total acceleration length, which is $240\,Z_R$. This justifies the lower-than-expected energy gain and the poorer energy spread.

In the first three simulations shown, those in Fig. 9, the efficiency from the laser to the accelerated electrons is about 5.5%, as in the simulation designs in Table 3. In the 27-GeV simulation the efficiency is reduced to 3.7%, and in the 95-GeV simulation it is only 2.5%. The reduction in efficiency for the 27-GeV and 95-GeV simulations is due to the smaller charge used to compensate for the weakening of the normalized wakefield in these cases. The acceleration length used in all simulations was $L_{\phi,b}$, therefore $\eta \lesssim \frac{1}{3a_0} = \frac{1}{6}$. In addition to this, the beam loading efficiency in these simulations was only a fraction of the ideal 100%. All of these factors contributed to the efficiencies – both proposed in Table 3 and measured from simulation

https://doi.org/10.1017/S0022377812000232 Published online by Cambridge University Press

– being about 5%. Parameter scans with QuickPIC can allow us to study longer propagation distances, increase the total charge, improve the beam quality, and raise the accelerator efficiency to about 10%.

5. Conclusions

Laser wakefield accelerators yield energetic electrons in very short distances, and with careful choice of the accelerator parameters this process can efficiently produce high-quality beams. To demonstrate this, we used scaling laws and the PIC code QuickPIC. We developed a parameter design in the weakly relativistic regime, where the laser power is equal to the critical power for self-focusing, and verified it with simulations. In doing so, the scaling formulas by Lu et al. (2007) were confirmed for electron beams that reach energy up to 95 GeV. In the simulations, laser guiding by a combination of self-guiding and external guiding was also demonstrated for over 240 Rayleigh lengths. These simulations resulted in beams with low energy spread, around 1%, and efficiency around 5% (from the laser pulse to the electron beam). Low energy spread was maintained throughout the acceleration process, using externally injected beams with ordinary Gaussian charge profile, for which we specified the length and the total charge. Under these conditions, reaching dephasing is inconsequential to the beam quality.

To perform these simulations we benchmarked QuickPIC extensively against the full-PIC code OSIRIS, and showed that in the weakly relativistic regime it is possible to use QuickPIC for the entire acceleration process and achieve a speed-up of more than 3 orders of magnitude. This opens the way for studying many physical effects, especially those arising from imperfections of the laser pulse or the electron beam.

These simulations were carried out several years ago (Tzoufras 2008). Recently, improvements have been made to QuickPIC, which have increased its speed and accuracy (An 2011, private communication). These improvements will be integrated into the laser solver, and when they do, they will permit modeling of accelerating stages with energies in excess of 100 GeV with speedup 10^5 compared with conventional PIC.

Acknowledgements

We acknowledge useful discussions with Drs. W. Lu and B. Cowan. This work was supported by DOE under grants DE-FC02-07ER41500, DE-FG02-02FR40727, DE-FG02-03ER54721, and DE-FG52-09NA29552, and NSF under NSF grants PHY090439 and PHY0321345.

References

Decker, C. D., Mori, W. B., Tzeng, K.-C. and Katsouleas, T. 1996 The evolution of ultra-intense, short-pulse lasers in underdense plasmas. *Phys Plasmas* **3**(5), 2047–2056.

Esarey, E., Sprangle, P., Krall, J. and Ting, A. 1996 Overview of plasma-based accelerator concepts. *IEEE Trans. Plasma Sci.* **24**(2), 252–288.

Esarey, E., Sprangle, P., Krall, J. and Ting, A. 1997 Self-focusing and guiding of short laser pulses in ionizing gases and plasmas. *IEEE J. Quantum Electron.* **33**(11), 1879 –1914.

Faure, J., Glinec, Y., Pukhov, A., Kiselev, S., Gordienko, S., Lefebvre, E., Rousseau, J. P., Burgy, F. and Malka, V. 2004 A laser-plasma accelerator producing monoenergetic electron beams. *Nature* **431**(7008), 541–544.

Faure, J., Rechatin, C., Norlin, A., Lifschitz, A., Glinec, Y. and Malka, V. 2006 Controlled injection and acceleration of electrons in plasma wakefields by colliding laser pulses. *Nature* **444**(7120), 737–739.

Fonseca, R. A., Martins, S. F., Silva, L. O., Tonge, J. W., Tsung, F. S. and Mori, W. B. 2008 One-to-one direct modeling of experiments and astrophysical scenarios: pushing the envelope on kinetic plasma simulations. *Plasma Phys. Control. Fusion* **50**(12), 124034.

Fonseca, R. A., Silva, L. O., Tsung, F. S., Decyk, V. K., Lu, W., Ren, C., Mori, W. B., Deng, S., Lee, S., Katsouleas, T., et al. 2002 Osiris: a three-dimensional, fully relativistic particle in cell code for modeling plasma-based accelerators. In: *Proceedings of International Conference on Computational Science – ICCS 2002, Amsterdam, The Netherlands*, April 21–24, 2002, Part III (eds. P. M. A. Sloot, C. J. K. Tan, J. Dongarra and A. G. Hoekstra), Lecture Notes in Computer Science, vol. 2331. Springer, Berlin, Germany, pp. 342–351.

Geddes, C. G. R., Toth, C., van Tilborg, J., Esarey, E., Schroeder, C. B., Bruhwiler, D., Nieter, C., Cary, J. and Leemans, W. P. 2004 High-quality electron beams from a laser wakefield accelerator using plasma-channel guiding. *Nature* **431**(7008), 538–541.

Gordon, D. F., Hafizi, B., Hubbard, R. F., Peñano, J. R., Sprangle, P. and Ting, A. 2003 Asymmetric self-phase modulation and compression of short laser pulses in plasma channels. *Phys. Rev. Lett.* **90**(21), 215001.

Huang, C., Decyk, V. K., Ren, C., Zhou, M., Lu, W., Mori, W. B., Cooley, J. H., Antonsen, Jr., T. M. and Katsouleas, T. 2006 Quickpic: a highly efficient particle-in-cell code for modeling wakefield acceleration in plasmas. *J. Comput. Phys.* **217**(2), 658–679.

Kalmykov, S. Y., Yi, S. A., Beck, A., Lifschitz, A. F., Davoine, X., Lefebvre, E., Khudik, V., Shvets, G. and Downer, M. C. 2011 Dark-current-free petawatt laser-driven wakefield accelerator based on electron self-injection into an expanding plasma bubble. *Plasma Phys. Control. Fusion* **53**(1), 014006.

Lu, W., Huang, C., Zhou, M., Mori, W. B. and Katsouleas, T. 2006a Nonlinear theory for relativistic plasma wakefields in the blowout regime. *Phys. Rev. Lett.* **96**(16), 165002.

Lu, W., Huang, C., Zhou, M., Tzoufras, M., Tsung, F. S., Mori, W. B. and Katsouleas, T. 2006b A nonlinear theory for multidimensional relativistic plasma wave wakefields. *Phys. Plasmas* **13**(5), 056709.

Lu, W., Tzoufras, M., Joshi, C., Tsung, F. S., Mori, W. B., Vieira, J., Fonseca, R. A. and Silva, L. O. 2007 Generating multi-gev electron bunches using single stage laser wakefield acceleration in a 3D nonlinear regime. *Phys. Rev. ST Accel. Beams* **10**(6), 061301.

Mangles, S. P. D., Murphy, C. D., Najmudin, Z., Thomas, A. G. R., Collier, J. L., Dangor, A. E., Divall, E. J., Foster, P. S., Gallacher, J. G., Hooker, C. J., et al. 2004

https://doi.org/10.1017/S0022377812000232 Published online by Cambridge University Press

Monoenergetic beams of relativistic electrons from intense laser-plasma interactions. *Nature* **431**(7008), 535–538.

Martins, S. F., Fonseca, R. A., Lu, W., Mori, W. B. and Silva, L. O. 2010 Exploring laser-wakefield-accelerator regimes for near-term lasers using particle-in-cell simulation in lorentz-boosted frames. *Nat. Phys.* **6**(4), 311–316.

Michel, P., Schroeder, C. B., Shadwick, B. A., Esarey, E. and Leemans, W. P. 2006 Radiative damping and electron beam dynamics in plasma-based accelerators. *Phys. Rev.* E **74**(2), 026501.

Mora, P. and Antonsen, Jr., T. M. 1997 Kinetic modeling of intense, short laser pulses propagating in tenuous plasmas. *Phys. Plasmas* **4**(1), 217–229.

Mori, W. B. 1997 The physics of the nonlinear optics of plasmas at relativistic intensities. *IEEE J. Quantum Electron.* **33**(11), 1942–1953.

Pak, A., Marsh, K. A., Martins, S. F., Lu, W., Mori, W. B. and Joshi, C. 2010 Injection and trapping of tunnel-ionized electrons into laser-produced wakes. *Phys. Rev. Lett.* **104**(2), 025003.

Pollock, B. B., Clayton, C. E., Ralph, J. E., Albert, F., Davidson, A., Divol, L., Filip, C., Glenzer, S. H., Herpoldt, K., Lu, W., et al. 2011 Demonstration of a narrow energy spread, ~ 0.5 *gev* electron beam from a two-stage laser wakefield accelerator. *Phys. Rev. Lett.* **107**(4), 045001.

Pukhov, A. and Gordienko, S. 2006 Bubble regime of wake field acceleration: similarity theory and optimal scalings. *Phil. Trans. R. Soc.* **A 364**(1840), 623–633.

Rechatin, C., Faure, J., Davoine, X., Lundh, O., Lim, J., Ben-Ismaïl, A., Burgy, F., Tafzi, A., Lifschitz, A., Lefebvre, E., et al. 2010 Characterization of the beam loading effects in a laser plasma accelerator. *New J. Phys.* **12**(4), 045023.

Sprangle, P., Esarey, E. and Ting, A. 1990 Nonlinear interaction of intense laser pulses in plasmas. *Phys. Rev.* A **41**(8), 4463–4469.

Tajima, T. and Dawson, J. M. 1979 Laser electron accelerator. *Phys. Rev. Lett.* **43**(4), 267–270.

Tsung, F. S., Lu, W., Tzoufras, M., Mori, W. B., Joshi, C., Vieira, J. M., Silva, L. O. and Fonseca, R. A. 2006 Simulation of monoenergetic electron generation via laser wakefield accelerators for 5-25 tw lasers. *Phys. Plasmas* **13**(5), 056708.

Tzoufras, M. 2008 *Generation of Multi-Giga-Electron-Volt Monoenergetic Electron Beams via Laser Wakefield Acceleration*, ProQuest, UMI Dissertation, Ann Arbor, MI.

Tzoufras, M., Lu, W., Tsung, F. S., Huang, C., Mori, W. B., Katsouleas, T., Vieira, J., Fonseca, R. A. and Silva, L. O. 2008 Beam loading in the nonlinear regime of plasma-based acceleration. *Phys. Rev. Lett.* **101**(14), 145002.

Tzoufras, M., Lu, W., Tsung, F. S., Huang, C., Mori, W. B., Katsouleas, T., Vieira, J., Fonseca, R. A. and Silva, L. O. 2009 Beam loading by electrons in nonlinear plasma wakes. *Phys. Plasmas* **16**(5), 056705.

Vieira, J., Fiuza, F., Fonseca, R. A., Silva, L. O., Huang, C. K., Lu, W., Tzoufras, M., Tsung, F. S., Decyk, V., Mori, W. B., et al. 2008 One-to-one full-scale simulations of laser-wakefield acceleration using quickpic. *IEEE Trans. Plasma Sci.* **36**(4), 1722–1727.

Vieira, J., Fiúza, F., Silva, L. O., Tzoufras, M. and Mori, W. B. 2010 Onset of self-steepening of intense laser pulses in plasmas. *New J. Phys.* **12**(4), 045025.

Vieira, J., Martins, S. F., Pathak, V. B., Fonseca, R. A., Mori, W. B. and Silva, L. O. 2011 Magnetic control of particle injection in plasma based accelerators. *Phys. Rev. Lett.* **106**, 225001.

https://doi.org/10.1017/S0022377812000232 Published online by Cambridge University Press